

1 **Dynamics of bacterial communities and substrate conversion during olive-mill**  
2 **waste dark fermentation: prediction of the metabolic routes for hydrogen**  
3 **production**

4

5 Gianmarco Mugnai<sup>1</sup>, Luigimaria Borruso<sup>2</sup>, Tanja Mimmo<sup>2</sup>, Stefano Cesco<sup>2</sup>, Vincenzo  
6 Luongo<sup>3</sup>, Luigi Frunzo<sup>3</sup>, Massimiliano Fabbricino<sup>4</sup>, Francesco Pirozzi<sup>4</sup>, Francesca  
7 Cappitelli<sup>1</sup>, Federica Villa<sup>1\*</sup>

8

9 <sup>1</sup> Department of Food, Environmental and Nutritional Sciences, University of Milan, via  
10 Celoria 2, 20133 Milan, Italy

11 <sup>2</sup> Faculty of Science and Technology, Free University of Bolzano, Piazza Università 5,  
12 39100 Bolzano, Italy

13 <sup>3</sup> Department of Mathematics and Applications “Renato Caccioppoli”, University of  
14 Naples “Federico II”, via Cintia, Monte S. Angelo, 80126 Naples, Italy

15 <sup>4</sup> Department of Civil, Architectural and Environmental Engineering, University of  
16 Naples “Federico II”, via Claudio 21, 80125 Naples, Italy

17

18 \* Corresponding author: Prof. Federica Villa, [federica.villa@unimi.it](mailto:federica.villa@unimi.it). Department of  
19 Food, Environmental and Nutritional Sciences, University of Milan, via Celoria 2,  
20 20133 Milan, Italy.

21

22 **Abstract**

23 The aim of this work was to study the biological catalysts and possible substrate  
24 conversion routes in mesophilic dark fermentation reactors aimed at producing H<sub>2</sub> from  
25 olive mill wastewater. *Bacillus* and *Clostridium* were the most abundant phylotypes  
26 during the rapid stage of H<sub>2</sub> production. Chemical analyses combined with predictive

27 functional profiling of the bacterial communities indicated that the lactate fermentation  
28 was the main H<sub>2</sub>-producing route. In fact, during the fermentation process, lactate and  
29 acetate were consumed, while H<sub>2</sub> and butyrate were being produced. The fermentation  
30 process was rich in genes that encode enzymes for lactate generation from pyruvate.  
31 Lactate conversion to butyrate through the generation of pyruvate produced H<sub>2</sub> through  
32 the recycling of electron carriers via the pyruvate ferredoxin oxydoreductase pathway.  
33 Overall, these findings showed the synergy among lactate-, acetate- and H<sub>2</sub>-producing  
34 bacteria, which complex interactions determine the H<sub>2</sub> production routes in the  
35 bioreactors.

36

37 **Keywords:** Olive-mill waste dark fermentation, Biohydrogen, Bacterial Community,  
38 Metabolic route, Lactate fermentation

39

## 40 **1. Introduction**

41 The cultivation of olive plants and the production of olive oil have deep roots in the  
42 history of the Mediterranean basin. Olive oil production represents a very important  
43 agro-industrial activity for many countries, primarily Spain, Italy, Greece and Portugal,  
44 followed by Turkey, Morocco, Algeria and Tunisia. The production from these  
45 countries reaches more than 3.14 billion tons in 2019/2020  
46 (<http://www.internationaloliveoil.org>). Countries outside the Mediterranean region, such  
47 as Argentina, Australia, the US, South Africa and countries in the Middle East are the  
48 emerging olive oil producers. Over the last decade, olive oil has become an increasingly  
49 valuable source of antioxidant, anti-inflammatory, anti-proliferative, anti-atherogenic  
50 and essential fatty acid for the human diet, representing one of the most important  
51 dietary trends worldwide (Dermeche et al., 2013). Thus, the market for olive oil is

52 growing at a rapid pace owing to the surging demand from consumers for the nutritional  
53 values of olive oil.

54 However, the continuous expansion of the olive oil production is accompanied by the  
55 generation of huge amount of wastes, which include 30 million m<sup>3</sup> per year of olive mill  
56 wastewater (OMW) with a high pollutant load (Meftah et al., 2019). OMW is a  
57 challenging waste to treat because of its own characteristics, such as high salt  
58 concentration (EC 5-10 mS cm<sup>-1</sup>), high acidity (pH 4-5), high biological and chemical  
59 oxygen demand (BOD and COD of 100,000 and 220,000 mg L<sup>-1</sup>, respectively), and  
60 high content of polyphenols (Aharonov-Nadborny et al., 2018). The disposal of  
61 untreated OMW is a major environmental issue in the Mediterranean countries, where  
62 olive oil production is large and concentrated in a relatively short period. The  
63 uncontrolled OMW disposal is phytotoxic and it affects microbial activity,  
64 biogeochemical cycles of nutrients, pH and the salinity of both soil and water (Doula et  
65 al., 2017). Therefore, new treatments for the management and disposal of this waste are  
66 urgently needed. Nowadays, the valorization of OMW, while simultaneously degrading  
67 pollutants and producing green energy, is receiving a great attention. Indeed, the current  
68 trend is to obtain the energy directly from OMW in the form of hydrogen (H<sub>2</sub>), rather  
69 than to spend the extra energy to treat the waste. There are several routes for H<sub>2</sub>  
70 production from OMW, such as photobiological processes (Pintucci et al., 2015), dark  
71 fermentation processes (Scoma et al., 2013; Ghimire et al., 2015 and 2016),  
72 bioelectrochemical systems (Lin et al., 2014) and a steam reforming reaction (Rocha et  
73 al., 2017). Among the aforementioned routes, dark fermentation process is attractive  
74 because of the wide-range operational temperatures and pressures, the possible usage of  
75 various organic wastes, and the recovery of both the energy and the fermentation by-  
76 products (Ghimire et al., 2015). However, the literature data on OMW dark  
77 fermentation are scarce. Scoma et al. (2013) demonstrated that the production of biofuel

78 and bio-based chemicals from de-phenolized OMW under dark fermentative conditions  
79 in packed bed biofilm reactors depends on the applied hydraulic retention time. Ghimire  
80 and colleagues (2015) reported that the H<sub>2</sub> potential of OMW was 46 mL H<sub>2</sub> per gram  
81 of VS, and that the H<sub>2</sub> yield doubled when the activated sludge that had been pre-treated  
82 with heat shock was used as inoculum (Ghimire et al., 2016).

83 Hydrogenases are the main enzyme that regulates the H<sub>2</sub> metabolism and they are  
84 classified into three groups based on the number and identity of the metal in their active  
85 sites, such as nickel-iron [NiFe], iron-irons [FeFe] and iron [Fe] hydrogenases (Łukajtis  
86 et al., 2018). H<sub>2</sub>-producing proteins are linked to the efficiency of dark fermentative H<sub>2</sub>  
87 production and also to the bacteria involved in the process (Kothari et al., 2017).

88 Hydrogen is produced by a wide variety of obligate anaerobic and facultative anaerobic  
89 microorganisms that plays an essential role in the dark fermentation process. Among the  
90 microorganisms that strictly require anaerobic conditions, *Clostridium* species are key  
91 players in H<sub>2</sub> production due to their ability to utilize a wide range of substrates (Cabrol  
92 et al., 2017). *Clostridium* are able to harvest the electrons from pyruvate oxidation and  
93 to use these electrons for the oxidation of reduced ferredoxin by an [FeFe] hydrogenase,  
94 generating H<sub>2</sub> through the pyruvate ferredoxin oxydoreductase (PFOR) pathway (Cabrol  
95 et al., 2017). Facultative anaerobes such as *Enterobacter* species produce biogas  
96 through pyruvate-formate-lyase (PFL) pathway, in which formate is split into H<sub>2</sub> and  
97 CO<sub>2</sub> by a [NiFe] hydrogenase complex (Cabrol et al., 2017).

98 Despite few papers have dealt with H<sub>2</sub> production through dark fermentation of OMW,  
99 none of them identified the bacteria responsible for H<sub>2</sub> production and their partnerships  
100 with other anaerobic microorganisms. Furthermore, the main pathways for H<sub>2</sub>  
101 production in the olive-mill waste dark fermentation processes is still unknown.

102 The objective of this work was to uncover the biological catalysts (the key players of  
103 the bacterial community) and possible substrate conversion routes in mesophilic dark

104 fermentation reactors aimed at producing H<sub>2</sub> from OMW. The approach adopted was  
105 twofold: i) to investigate the temporal dynamics of both bacterial communities and  
106 metabolic profiles during the batch fermentation of OMW ii) to investigate the main  
107 bacterial partnerships for H<sub>2</sub> production via metagenome functional prediction.  
108 To this end, high-throughput 16S rRNA gene sequencing was used to unveil the key  
109 bacteria involved in the fermentation process. The taxonomic composition of the  
110 microbial assembly, the alpha- diversity of the microflora, and the fermentation  
111 products were analyzed. Finally, fermentation products analyses and predictive  
112 functional profiling were performed to study the relationships between process  
113 performance indicators and the bacterial community activity. This is the first study  
114 reporting the possible metabolic routes responsible for H<sub>2</sub> production in an OMW  
115 fermentation system from a microbiological perspective.

116

## 117 **2. Materials and methods**

### 118 **2.1. Olive mill waste and inoculum characterization**

119 Olive mill waste (OMW) samples were obtained from the “Fasano oil mill” located in  
120 Salerno, Italy. The chemical oxygen demand (COD) method was used to determine the  
121 OMW carbon content. The value of 138.75 gO<sub>2</sub> L<sup>-1</sup> was obtained and used for set-up  
122 purposes. Total solids (TS), volatile solids (VS), and total kjeldahl nitrogen (TKN) of  
123 the OMW were 8.1 gTS L<sup>-1</sup>, 4.9 gVS L<sup>-1</sup>, and 0.45 g L<sup>-1</sup>, respectively. COD, TS, VS  
124 and TKN were measured as described in the Standard Methods (APHA, 2005). A more  
125 complete characterization of the OMW can be found in Ghimire et al. (2016), where a  
126 similar wastewater from the same oil mill was used. The substrate was stored at -20°C  
127 in lab refrigerators. The initial pH of 5.3 was measured for all OMW samples. The pH  
128 value was checked prior to each experiment and a constant trend was monitored over  
129 time.

130 The anaerobic digestate used as inoculum for dark fermentation tests was obtained from  
131 a local full-scale anaerobic reactor treating cow sewage (Salerno, Italy). The inoculum  
132 characterization highlighted the VS content of 47.76 gVS L<sup>-1</sup>. This value was converted  
133 in soluble COD by using the empirical conversion rate of 1.48 gO<sub>2</sub> gVS<sup>-1</sup> usually  
134 adopted in wastewater treatment for activated sludge. The pH of the inoculum was 7.8.  
135 The substrate to inoculum ratio (food to microorganisms, F/M) was fixed at 2 gCOD  
136 gVS<sup>-1</sup> as operational condition to produce a significant amount of H<sub>2</sub> under uncontrolled  
137 pH regimen (Spasiano et al., 2019).

138

### 139 **2.2. Dark fermentation experiments**

140 Batch experiments of dark fermentation were carried out using airtight 500-mL  
141 transparent borosilicate glass bottles (Schott Duran, Germany), placed in a thermostat-  
142 controlled water bath at 37°C (mesophilic conditions). To limit the activity of H<sub>2</sub>-  
143 consuming microorganisms, the inoculum was pre-treated at 105°C for 2h (Maharaj et  
144 al., 2019). The batch reactors were equipped with airtight caps fitted with sampling  
145 pipes for biogas, liquid mixtures, and organic acid. All the experiments were conducted  
146 in duplicate. Each experiment was stopped when H<sub>2</sub> production was no longer observed.

147

### 148 **2.3. Analytical methods**

149 The total volume of biogas (including H<sub>2</sub>, CO<sub>2</sub>, O<sub>2</sub> and N<sub>2</sub>), was measured using a gas  
150 chromatograph (GC) with argon as the gas carrier (Varian Star 3400, Varian Australia  
151 Pty Ltd., Victoria, Australia) equipped with a thermal conductivity detector. The GC  
152 was also equipped with a ShinCarbon ST 80/100 column (Restek Corporation,  
153 Bellafonte, PA, USA).

154 The organic acids (citrate, lactate, acetate, formate, butyrate, valerate and caproate)  
155 were analyzed by High Performance Liquid Chromatography (HPLC) using a Dionex

156 chromatograph (Dionex Corporation, Sunnyvale, CA, USA). The system consisted of a  
157 chromatography oven (Dionex LC 25) equipped with a Metrosep Organic Acids –  
158 250/7.8 column (Metrohm, Herisau, Switzerland) and an absorbance detector (Dionex  
159 AD25) connected to a gradient pump (Dionex GP 50). All samples were eluted with 0.5  
160 mmol L<sup>-1</sup> sulfuric acid pumped at 0.7 mL min<sup>-1</sup>. The pH was measured with a lab pH-  
161 meter (HI 98190 pH/ORP, Hanna Instruments, Woonsocket, RI, USA).

162

#### 163 **2.4. Bacterial community analyses**

164 Samples for bacterial community analyses were collected at: i) day 0 (T0),  
165 corresponding to the inoculum, ii) day 3 (T3), corresponding to the initial stage of  
166 hydrogen production, iii) day 5 (T5), corresponding to the rapid stage of hydrogen  
167 production, and iv) day 8 (T8), corresponding to the end of the dark fermentation. At  
168 least three biological replicates for each time points were taken and analyzed. Total  
169 genomic DNA was extracted according to the manufacturer's instructions from  
170 PowerBiofilm DNA Isolation Kit (MoBio Laboratories Inc., Carlsbad, CA). High-  
171 throughput sequencing analysis of the V3–V4 region of the bacterial 16S rRNA gene  
172 (primers CS1\_341F/CS2\_806R) was performed by using a MiSeq platform (Illumina)  
173 with v3 chemistry providing 2 × 300 paired-end read (Rapin et al., 2017).  
174 Raw data were preprocessed, quality filtered, trimmed, denoised , paired, and modeled  
175 via QIIME2 (Bolyen et al., 2019) and DADA2. Chimeras were detected using DADA2  
176 according to the “consensus” method. Sequences were clustered into Sequences  
177 Variants (SV). SVs were assigned using a Naïve-Bayes classifier trained on the SILVA  
178 database. Samples were rarefied at the minimum library size of 4464.  
179 All sequences were submitted to the European Nucleotide Archive (EMBL-EBI) under  
180 the accession numbers ERS4861634 - ERS4861650.

181

## 2.5. Data analyses

Multi packages of R software were used to perform the statistical analyses (R Core Team, 2017). Rarefaction curves were done using no-normalized SVs table. Alpha-diversity was calculated with Richness, Shannon index and Evenness using multi package of R software. The differences among samples were evaluated using ANOVA followed by the Turkey (HSD) test. In case of data not normally distributed, the Kruskal-Wallis test was applied and followed by the Dunn test. Co-occurrences among the most abundant bacterial genera (relative abundance >1%) was assessed by the Pearson correlation coefficient.

The modified Gompertz equation (1) was used to model biogas production during the fermentation process (Ghimire et al., 2015).

$$(1) H(t) = H_0 \exp \left\{ -\exp \left[ \frac{R}{H_0} (\lambda - t) + 1 \right] \right\}$$

In equation 1,  $H(t)$  is the cumulative gas production (mL),  $\lambda$  is the lag-phase time (h),  $H_0$  is the gas production potential (mL),  $R$  is the maximum gas production rate (mL day<sup>-1</sup>),  $t$  is the incubation time (day), and  $e$  is the  $\exp(1)=2.718$ . Parameters were estimated using the curve fit function in XLSTAT (Addinsoft, version 21.4.1).

H<sub>2</sub> yields were calculated by dividing the final cumulative H<sub>2</sub> produced by the amount of the VS added at the start of the experiment.

The maximum concentration of each metabolite was converted into COD (g O<sub>2</sub> L<sup>-1</sup>) by using the COD equivalent factors reported in Moscoviz et al. (2018). The OMW conversion efficiency was then calculated as a percentage by dividing this maximum concentration by the initial COD in the bioreactor.

The principal component analysis (PCA) on the correlation matrix was performed using the XLSTAT software to visualize the relationship between the dominant bacterial groups and the main metabolites over time. The first two PCs were subsequently plotted to visualize the results.



208

## 209 **2.6. Functional prediction analysis**

210 PICRUSt2 (Phylogenetic Investigation of Communities by Reconstruction of  
211 Unobserved States) that infer microbial gene content from 16S rRNA data was used to  
212 explore the potential functionality of the bacterial community (Langille et al., 2013).  
213 Functional gene prediction was obtained from KEGG-Orthology (KO). Besides,  
214 information on metabolic pathways and EC numbers involved in the dark fermentation  
215 were manually categorized based on the KEGG and BRENDA databases. Bacterial  
216 genera contributing to the genes involved in the main metabolic routes were further  
217 investigated by hidden state prediction.

218

## 219 **3. Results and Discussion**

### 220 **3.1. Dynamics of the bacterial community structure and diversity**

221 To gain insight into the dark fermentation process of OMW, the dynamics of the  
222 bacterial community structure was deeply investigated by 16S rRNA gene high-  
223 throughput sequencing.  
224 After bioinformatic analysis, a total of 1,355,103 reads assigned as Bacteria clustered in  
225 2,679 SVs with 99% similarity were found. Rarefaction curves showed that all the  
226 samples reached the plateau, indicating that the depth of the sampling and sequencing  
227 was sufficiently to detect a nearly maximum number of SVs.  
228 Diversity indices for the samples at different fermentation stages are shown in Figure  
229 1A. Richness, Shannon indices and Evenness showed stable trends over time. Since  
230 these indices are based on the DNA-sequencing results, it is reasonable to expect that  
231 any variation in the fermentation performance may result primarily from the changes in  
232 the functional activities of the established bacterial community (metabolically active

233 community), rather than the changes in alpha diversity of the total community (Klein et  
234 al., 2016).

235 As shown in Figure 1B, there were sixteen genera with a relative abundance higher than  
236 1% in the samples over time. The predominant phyla of the whole fermentation process  
237 were Firmicutes (78.58%), Cloacimonetes (4.70%), Actinobacteria (4.27%),  
238 Proteobacteria (4.11%) and Bacteroidetes (3.73%). The microbial community structure  
239 changed during the hydrogen fermentation process. At the inoculation stage T0, the  
240 most representative taxon was *Clostridium* (38.23%), followed by *Cloacimonadaceae*  
241 W5 (12.10%), *Corynebacterium* (9.64%), *Paenibacillus* (8.03%) and *Acinetobacter*  
242 (7.01%).

243 From T3, *Bacillus* became the most dominant genus with percentage values ranging  
244 from 30.61% to 23.07% of the total taxa, followed by *Clostridium* genus.

245 At T5, besides *Bacillus* and *Clostridium*, two other taxa belonging to the Cloacimonetes  
246 and Actinobacteria phyla were also dominant, namely *Cloacimonadaceae* W5 and  
247 *Corynebacterium*, respectively. At the end of the dark fermentation (T8), there was an  
248 enrichment of other genera, such as *Lysinibacillus* (6.51%), *Ruminiclostridium* (6.29%),  
249 *Corynebacterium* (6.16%) and *Caproiciproducens* (5.26%), as well as *Bacillus*  
250 (23.07%), *Clostridium* (17.19%) and *Cloacimonadaceae* W5 (14.65%). In this study,  
251 the *Clostridium* genus is referred to *Clostridium sensu stricto*, composed by 8 clusters:  
252 *Clostridium sensu stricto* 1, 3, 6, 7, 10, 12 (identified as *Clostridium butyrium*) and 13.  
253 Lactic acid bacteria (LAB) such as *Turicibacter* (Ikeda-Ohtsubo et al., 2018) and some  
254 species of Ruminococcaceae (Boonsaen et al., 2017) remained constant over time.

255 Overall, the findings showed the enrichment of potential HPB over time. Among HPB,  
256 *Clostridium* spp. are considered the most abundant and most efficient hydrogen  
257 producers in mesophilic fermentation processes. These bacteria are able to generate H<sub>2</sub>  
258 from different substrates, providing H<sub>2</sub> yields from 0.5 to 3 mol-H<sub>2</sub>/mol-hexose (Yang

259 and Wang, 2019; Yin and Wang, 2016). In batch experiments treating palm oil mill  
260 effluent inoculated with heat-shocked sludge pit, the increase of the H<sub>2</sub>-producing  
261 potential was strongly correlated to the microbial shift toward a *Clostridium* spp.-  
262 dominated community (Maaroff et al., 2019).

263 The most abundant cluster of *Clostridium sensu stricto* genus was *Clostridium sensu*  
264 *stricto* 1. The dominance of this genus was demonstrated also in other research of H<sub>2</sub>  
265 production via the dark fermentation (Yang et al., 2019; Yang and Wang, 2019). In  
266 addition, *Clostridium sensu stricto* 7, the second most-common cluster, was also found  
267 in batch experiments of sludge and flower waste co-fermentation aimed at producing H<sub>2</sub>  
268 (Yang and Wang, 2018).

269 Some spore-forming facultative anaerobic Bacillales have been reported to produce H<sub>2</sub>  
270 through the formate hydrogen lyase pathway, providing high yields around 2 mol-  
271 H<sub>2</sub>/mol-hexose (Cabrol et al., 2017). Compared to *Clostridium*, *Bacillus* spp. are less  
272 sensitive to oxygen and they contribute in creating the anaerobic conditions suitable for  
273 the growth of strict anaerobic HPB. In fact, at the beginning of the batch fermentation  
274 process, the oxygen in the reactor headspace can solubilize in the bulk liquid, favoring  
275 the activities of *Bacillus* spp.

276 *Romboutsia* and *Sedimentibacter* were common taxa found in H<sub>2</sub> production studies  
277 using heat shock pre-treated inoculum (Yang et al., 2019; Yang and Wang, 2019).

278 Although Proteobacteria represent a small proportion of the whole phyla, the presence  
279 of *Acinetobacter* increase during the dark fermentation process. Yang and Wang (2018)  
280 reported that this taxon has an important role in H<sub>2</sub> production and consumption during  
281 the dark fermentation process.

282 *Caproiciproducens* increased significantly during the dark fermentation process.  
283 According to Feng et al. (2018), the presence of *Caproiciproducens* was related to the  
284 production of acetate, butyrate and H<sub>2</sub>. *Ruminofilibacter* (Bacteroidetes phylum) is a

285 rumen bacterium that has been detected earlier in a mesophilic anaerobic reactor. This  
286 genus is considered as a degrader of lignocellulosic materials.

287 Beside the presence of well-known HPB in the mesophilic fermentative microbiota, it is  
288 important to note the crucial role of auxiliary bacteria that are not necessarily involved  
289 in primary H<sub>2</sub> production, but rather tightly interacting (either positively or negatively)  
290 with HPB, resulting in variable functional outcomes. In fact, the presence of these  
291 microorganisms can enhance or discourage H<sub>2</sub> production through different  
292 mechanisms, such as cometabolism, oxygen consumption, pH regulation, substrate  
293 hydrolysis and cell aggregation (Cabrol et al., 2017).

294 In order to investigate the interactive structure of the fermentative community, Pearson  
295 correlations between microbial abundances was performed as shown in Figure 2.

296 The Pearson's correlation analysis between the dominant bacterial groups during the  
297 dark fermentation process revealed that both *Bacillus* and *Clostridium* were positively  
298 correlated to *Lachnoclostridium* ( $r_{Bacillus} = 0.78$ ,  $p_{Bacillus} < 0.001$ ;  $r_{Clostridium} = 0.63$ ,  
299  $p_{Clostridium} = 0.006$ ), *Acinetobacter* ( $r_{Bacillus} = 0.76$ ,  $p_{Bacillus} < 0.001$ ;  $r_{Clostridium} = 0.51$ ,  
300  $p_{Clostridium} = 0.036$ ) and *Caproiciproducens* ( $r_{Bacillus} = 0.65$ ,  $p_{Bacillus} = 0.005$ ;  $r_{Clostridium} =$   
301  $0.52$ ,  $p_{Clostridium} = 0.030$ ). *Lachnoclostridium* and *Caproiciproducens* are two well-  
302 characterized carbohydrate fermenters that used [FeFe]-hydrogenase for H<sub>2</sub> production  
303 (Greening et al., 2018). They are also major butyrate-producing bacteria (Gutiérrez and  
304 Garrido 2019), sustaining the activity of other HPB that can use a butyrate-type  
305 fermentation, where only the production of butyrate ensures the pathways to shift  
306 towards the H<sub>2</sub> production. *Acinetobacter* is a genus of Gram-negative bacteria  
307 belonging to the class of Gammaproteobacteria that are involved in multiple processes  
308 during the H<sub>2</sub> production. *Acinetobacter* not only is directly responsible for H<sub>2</sub>  
309 production (Kanchanasuta et al., 2017), but also for the degradation of hemicellulose  
310 and lignocellulosic materials contained in the OMW. Due to their ability to secrete high

311 quantities of hydrolytic enzymes such as xylanases and cellulases, *Acinetobacter* is  
312 implicated in the production of xylooligosaccharides (Purohit et al., 2017), providing  
313 substrate hydrolysis for other HPB. The positive correlation between *Acinetobacter* and  
314 the two main HPB explains the capability of both *Clostridium* and *Bacillus* to use the  
315 products of *Acinetobacter* transformation to produce H<sub>2</sub>, thus generating a metabolic  
316 synergy between hydrolyzers and HPB (de Sá et al., 2020).

317 *Lachnoclostridium*, *Acinetobacter* and *Bacillus* showed a positive correlation with  
318 *Paenibacillus* ( $r_{Lachnoclostridium} = 0.88$ ,  $p_{Lachnoclostridium} < 0.001$ ;  $r_{Acinetobacter} = 0.74$ ,  
319  $p_{Acinetobacter} < 0.001$ ;  $r_{Bacillus} = 0.81$ ,  $p_{Bacillus} < 0.001$ ). *Paenibacillus* is able to produce  
320 large amount of exopolysaccharides by utilizing OMW as the sole carbon and energy  
321 sources, with a concomitant reduction in the toxicity of the waste (Dermeche et al.,  
322 2013). The reduction in OMW toxicity by *Paenibacillus* was mainly related to the high  
323 phenolic-degrading activity and the production of extracellular polysaccharide-  
324 degrading enzymes (Aguilera et al., 2008), which likely supported the growth of other  
325 microorganisms such as *Lachnoclostridium*, *Acinetobacter* and *Bacillus*. In addition,  
326 according to Aguilera et al. (2001), *Paenibacillus* seems to be involved in the  
327 production of acids rather than biogas from many carbohydrates. This means that  
328 *Paenibacillus* can contribute positively to hydrogen production in mixed culture  
329 fermentations by slightly acidifying the local environment, supporting the development  
330 and activity of HPB

331 The main HPBs *Clostridium* and *Bacillus* presented a negative correlation with  
332 *Ruminofilibacter* and *Romboutsia* ( $r_{Ruminofilibacter} = -0.83$ ,  $p_{Ruminofilibacter} < 0.001$ ;  $r_{Romboutsia}$   
333  $= -0.55$ ,  $p_{Romboutsia} = 0.026$ ;  $r_{Ruminofilibacter} = -0.58$ ,  $p_{Ruminofilibacter} = 0.015$ ;  $r_{Romboutsia} = 0.69$ , ;  
334  $p_{Romboutsia} = 0.002$ ). *Ruminofilibacter* is polysaccharide-degrading genus found in  
335 anaerobic digesters for methane production (Ince et al., 2020), while *Romboutsia* is a  
336 potential acetogens that grows autotrophically using H<sub>2</sub> as an energy source,

337 respectively (Gerritsen et al., 2014). The negative correlation with the main HPB  
338 suggested that these bacteria outcompete HPB for their substrates and directly consume  
339 H<sub>2</sub>.

340

### 341 **3.2. Metabolic dynamics of the bacterial community**

342 The temporal successions of the cumulative biogas and the main metabolic  
343 intermediates from OMW fermentation were investigated (Figure 3). Biogas production  
344 parameters (the gas production potential H<sub>0</sub> (mL), the maximum gas production rate R  
345 (mL d<sup>-1</sup>), the lag-phase time lambda (d) and the determination coefficient R<sup>2</sup>) measured  
346 by the modified Gompertz model were reported in Figure 3A-D. The yield of H<sub>2</sub>  
347 increased over time, showing a rapid production from T3 to T8 with a maximum H<sub>2</sub>  
348 production rate of 15 mL d<sup>-1</sup> and a H<sub>2</sub> production potential of 60.6 mL (R<sup>2</sup>= 0.978,  
349 Figure 3A). The researchers claimed that the low H<sub>2</sub> yield can be due to the presence of  
350 polyphenols, which might have an inhibitory effect on the reactor's microflora. The  
351 total biogas trend showed a gradual increase from T1 to T8, without methane generation  
352 (Figure 3B-4D). The maximum biogas production rate was 166.2 mL d<sup>-1</sup> with a biogas  
353 production potential of 664.6 mL (R<sup>2</sup>= 0.992). The maximum H<sub>2</sub> yield of 33.8 mL H<sub>2</sub>  
354 gVS<sup>-1</sup> was obtained. This value was similar to the H<sub>2</sub> yield of 33.1 mL H<sub>2</sub> gVS<sup>-1</sup> reported  
355 by Ghimire et al. (2016), where a similar OMW was used.

356 Figure 3E showed the trend of pH during the dark fermentation process. As reported in  
357 the graph, the pH value decreased over time from 7.1 at T0 to 6.5 at T5 with the  
358 formation of acidic metabolites. At the end of the dark fermentation (T8), the pH value  
359 kept stable at 6.1.

360 The formation of the main soluble metabolites during the dark fermentation process was  
361 also investigated (Figure 3F-I). Propionate, valerate and caproate were not detected in  
362 the mesophilic reactors. The results showed that lactate and acetate were the main

363 metabolites generated during the initial stage of H<sub>2</sub> production (T3). Among them,  
364 acetate was the dominant ones. The conversions of the initial COD to lactate, acetate  
365 and formate at T3 were 8.9, 16, and 0.15 %, respectively. During the stages T5-T8, the  
366 concentration of formate, butyrate and H<sub>2</sub> increased, while the concentration of lactate  
367 and acetate decreased. Once the lactate was depleted, butyrate formation and H<sub>2</sub>  
368 production also ceased, despite the acetate availability. The conversions of the initial  
369 COD to lactate, acetate, formate and butyrate at T5 were 1.25, 16.6, 0.22 and 7.66%,  
370 respectively. At the end of the dark fermentation (T8), the concentrations of lactate,  
371 acetate, formate and butyrate were 0, 5403, 0 and 1476 mg L<sup>-1</sup>, which corresponded to  
372 0%, 78%, 0% and 22% of the total detected soluble metabolites, respectively.

373 The dynamics of metabolites presented herein seems to indicate a fermentative H<sub>2</sub>  
374 production from lactate and acetate. The generation of H<sub>2</sub>, CO<sub>2</sub> accompanied with  
375 production of butyrate from lactate/acetate fermentation has been previously reported in  
376 several studies (*inter alia* Matsumoto and Nishimura 2007; Fuess et al., 2018). Acetate  
377 is not only a source of carbon and energy for many metabolic reactions, but it is also  
378 required as an electron acceptor in the lactate fermentation (Duncan et al., 2004). The  
379 conversion of lactate and acetate to butyrate and H<sub>2</sub> is an energetically favorable process  
380 (Duncan et al., 2004).

381 To provide reliable data to clarify the main conversion routes established in the  
382 fermentation system, the bacterial community structure was correlated with the major  
383 metabolic by-products through principal component analysis (PCA) (Figure 4).

384 According to the PCA, which explained 89% of the total variability, it was possible to  
385 clearly discern the four phases that characterized the fermentation process of OMW,  
386 from the inoculum (T0) to the H<sub>2</sub> production (T8). Thus, major changes in both  
387 metabolites and bacterial profiles were observed as a function of the incubation time.

388 At T0, a positive correlation with pH was exhibited by *Sedimentibacter*,  
389 *Corynebacterium* and *Ruminofilbacter*. The last two genera are involved in the  
390 conversion of carbohydrates and complex molecules into small organic acids that  
391 lowered the pH (Jin et al., 2019).

392 The T3 phase was mainly characterized by the production of lactate, which was closely  
393 matched by the presence of the LAB *Turicibacter* in the bacterial community.

394 The final stage T8 encompassed the production of H<sub>2</sub>, where lactate, acetate and  
395 formate were consumed while H<sub>2</sub> and butyrate were produced. In fact, lactate was  
396 negatively correlated with the production of H<sub>2</sub> and butyrate. The observed trend  
397 indicated a H<sub>2</sub> production through a lactate fermentation (equation 2-3). During lactate  
398 fermentation electrons are transferred to either ferredoxin or NAD<sup>+</sup>, which favor H<sub>2</sub>  
399 production through proton reduction used to recycle the electron carriers (equation 2).

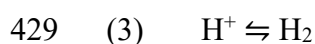
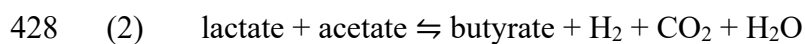
400 Excess NADH generated by the system is used to produce other reduced fermentation  
401 products, such as butyrate (Cabrol et al., 2017). The PCA biplot showed a positive  
402 correlation between butyrate and *Clostridium* genus. The ability to produce H<sub>2</sub> from  
403 lactate and acetate seems to be widely conserved in the genus *Clostridium* and other  
404 HPB capable of butyrate fermentation of carbohydrates (Matsumoto and Nishimura  
405 2007; Juang et al. 2011; Tao et al., 2016).

406 It is worth noting that the presence of formate was inversely correlated to lactate. The  
407 detection of formate at T5 (Figure 3H) suggested that, in the bioreactor, formate was  
408 produced by more than one group of bacteria via interconversion reactions, in addition  
409 to its direct conversion from glucose. This result supported the fact that lactate-based  
410 metabolic pathway might indirectly produce formate, which can split into H<sub>2</sub> and CO<sub>2</sub>  
411 through the PFL pathways (Cabrol et al., 2017). Indeed, formate positively correlated  
412 with the biogas production. Interestingly, acetate was inversely correlated with H<sub>2</sub> and  
413 butyrate production along the F2 axes. It should be noted that acetate is a substrate and



414 an intermediate of the lactate pathway in the butyrate transformation (equation 1)  
415 (Duncan et al., 2004). Several studies reported the stimulation of H<sub>2</sub> production by  
416 lactate and acetate mixed with the substrate. Baghchehsaraee et al. (2009) showed that  
417 the addition of lactate to a mixed culture grown on starch-containing medium increased  
418 both the H<sub>2</sub> production and the butyric acid formation. By contrast, when lactate was the  
419 only carbon source, the level of H<sub>2</sub> production was very low. Juang et al. (2011)  
420 observed the use of lactate and acetate for H<sub>2</sub> and butyrate production by mixed-bacteria  
421 culture from tapioca starch. Tao et al. (2016) claimed that exogenous acetate enhanced  
422 lactate conversion to butyrate at pH 6.0, whereas when fermentable lactate was omitted  
423 from the medium and acetate was used as a sole energy source, acetate was not  
424 consumed and butyrate was not produced. These findings suggest that the conversion of  
425 lactate and acetate into H<sub>2</sub> and butyrate is due to the cooperative interactions between  
426 lactate- and H<sub>2</sub>-producing bacteria.

427



430

### 431 **3.3. Predictive functional analysis of bacterial communities**

432 To deepen the understanding of the OMW fermentative ecosystems, it is crucial to  
433 know which substrate conversion pathways are operated by the bacterial community  
434 over time. In this study, the potential substrate conversion routes that might occur in the  
435 system and the contribution of the phylotypes to the main metabolic pathways were  
436 identified based on the functional genes predicted using the PICRUSt software.  
437 PICRUSt compares the identified 16S rRNA gene sequences to those of known species,  
438 thereby inferring the possible gene contents of the bacterial communities. Although  
439 PICRUSt results offer only a prediction, their combination with the temporal dynamic

440 of biogas production and metabolic intermediates can provide a clear idea of the  
441 possible metabolic activities in OMW dark fermentation.

442 Since H<sub>2</sub> can be produced by several different pathways, the presence and relative  
443 abundance of genes that code for the enzymes involved in the H<sub>2</sub> production from  
444 butyrate, acetate, formate and lactate were investigated. The predicted relative  
445 abundances of these genes, the main metabolic routes for H<sub>2</sub> production and their  
446 predicted metagenome contributions are summarized in Figure 5 and 6, respectively.

447 The fermentation process aimed at H<sub>2</sub> production was rich in genes that encode  
448 enzymes for lactate generation from pyruvate (L-lactate dehydrogenase (cytochrome),  
449 EC:1.1.1.27, n. 6; D-lactate dehydrogenase (cytochrome), EC:1.1.1.28, n. 3-4). The  
450 predicted main phylotypes that contribute to the presence of these lactate  
451 dehydrogenases were *Clostridium*, *Bacillus*, *Paenibacillus*, *Corynebacterium* and  
452 *Turicibacter*. The decreasing concentration of lactate during the fermentation process  
453 suggests its possible consumption through several interconversion reactions. The  
454 transformation of lactate to pyruvate was mainly operated by *Bacillus*, *Lysinibacillus*,  
455 *Rummeliibacillus* and *Corynebacterium* through the enzymes lactate dehydrogenases  
456 EC:1.1.2.4 (n. 2), and EC:1.1.2.3 (n. 5). The acetyl-CoA formed followed the metabolic  
457 pathways that produced mainly acetate and butyrate. These findings combined with the  
458 metabolite profiles reported in Figures 3 and 4 corroborate the contribution of lactate  
459 fermentation in the H<sub>2</sub> production. LAB have been detected in almost all of the  
460 fermentation systems aimed at producing H<sub>2</sub>. Although many studies have indicated that  
461 LAB inhibit H<sub>2</sub> production due to substrate competition and/or excretion of  
462 bacteriocines (Cabrol et al., 2017), positive interactions between LAB and clostridial  
463 species with production of H<sub>2</sub> from lactate have also been reported (Fuess et al., 2018;  
464 García-Depraect et al., 2019). Hydrogen production from lactate fermentation represents  
465 an important strategy that enable lactate-consuming HPB to obtain energy under

466 unfavorable conditions such as low carbohydrate-availability (García-Depraect et al.,  
467 2019). This is not the case of OMW, which are characterized by high chemical (COD)  
468 and biochemical oxygen demand (BOD) values. However, OMW are characterized by  
469 high concentrations of phenolic compounds that can be toxic for the microorganisms,  
470 with negative impacts on the fermentation process (Vavouraki et al., 2019). LAB can  
471 easily metabolize phenolic compound by either detoxifying or utilizing them as an  
472 alternative source of energy (Filannino et al., 2014).

473 The predicted relative abundance of the genes that encode key enzymes for acetate  
474 production and consumption (e.g. acetate kinase, EC:2.7.2.1, n. 14; phosphate  
475 acetyltransferase, EC:2.3.1.8, n. 15) was high throughout the fermentation process. The  
476 decreasing acetate concentration over time suggests that the consumption of acetate for  
477 several purposes, including the generation of energy and the production of other fatty  
478 acids. The main phylotypes associated to acetate production and/or consumption were  
479 *Bacillus*, *Corynebacterium*, *Paenibacillus Ruminococcaceae* UCG-014 and  
480 *Lysinibacillus*. These phylotypes may supply extra acetate that acts as an oxidizing  
481 agent for the bioconversions of lactate into H<sub>2</sub> (García-Depraect et al., 2019).

482 *Bacillus*, *Caproiciproducens*, *Clostridium*, *Lysinibacillus* and *Romboutsia*, were the  
483 principal phylotypes contributing to the presence of butyrate kinase (EC:2.7.2.7, n. 29)  
484 and acetate CoA-transferase (EC:2.8.3.8, n. 30-31), key enzymes that catalyze the  
485 conversion of butyrate phosphate and butyryl CoA to butyrate. In addition, based on the  
486 high butyrate and the decreasing of lactate and acetate concentrations over time, these  
487 bacteria may have produced butyrate via the lactate and acetate interconversion  
488 reactions.

489 Formate production and consumption are controlled by the key enzyme formate C-  
490 acetyltransferase (EC:2.3.1.54, n. 33), which belonged to the genus *Caproiciproducens*,  
491 *Clostridium*, *Lachnoclostridium*, *Romboutsia* and *Ruminiclostridium*.

492 An observation that is worth noting is that the H<sub>2</sub> production occurred mainly through  
493 the oxidation of reduced ferredoxin with a monomeric ferredoxin-dependent  
494 hydrogenase (hydrogen:ferredoxin oxidoreductase, EC:1.12.7.2, n. 20). Moreover,  
495 NADH was oxidized and the ferredoxin reduced by NADH:ferredoxin oxidoreductase  
496 (NFOR, EC 1.18.1.3, n. 21). The reduced ferredoxin can be used by electron bifurcating  
497 or monomeric ferredoxin-dependent hydrogenase to reduce protons, yielding H<sub>2</sub>. Both  
498 the above-mentioned enzymes belong to the PFOR pathway that is used by obligate  
499 anaerobic microorganisms to couple H<sub>2</sub> production to the recycling of the electron  
500 carriers ferredoxin and NADH that accumulate during the anaerobic metabolisms  
501 (Cabrol et al., 2017). The only two principal phylotypes carrying both the  
502 hydrogen:ferredoxin oxidoreductase and the NADH:ferredoxin oxidoreductase were  
503 *Clostridium* and *Romboutsia*. The PCA graph in Figure 4 showed a positive correlation  
504 between H<sub>2</sub> and *Clostridium*, while H<sub>2</sub> and *Romboutsia* are inversely related. This result  
505 suggested that the gut bacterium *Romboutsia* might act as a H<sub>2</sub> -consuming bacterium,  
506 which would contribute in explaining the low H<sub>2</sub> production in the bioreactors.  
507 *Romboutsia* is a potential acetogens that grows autotrophically using H<sub>2</sub> as an energy  
508 source (Gerritsen et al., 2014).

509 The PiCRUST analysis also predicted the H<sub>2</sub> production through the PFL pathway,  
510 where the formate is split into H<sub>2</sub> and CO<sub>2</sub> by a formate-hydrogen-lyase complex that  
511 contains a nickel-iron [NiFe] hydrogenase. However, the predicted abundance of the  
512 genes that code for the formate-hydrogen-lyase complex (EC:1.12.1.2, n. 40) was close  
513 to zero throughout the fermentation process and present in few rare bacterial species  
514 with relative abundance < 0.5%. Hence, on the basis of the metabolic predictions, the  
515 H<sub>2</sub> production through the PFL pathways was not an important metabolic reaction in the  
516 OMW fermentation reactors.

517 Figure 6 summarizes the prediction of the principal phylotypes at genus level that  
518 contribute to the genes that code for the key enzymes involved in the production and  
519 consumption of lactate, acetate, formate, butyrate, and H<sub>2</sub>. In the bioreactor, a  
520 collaboration between the bacteria that were involved in lactate (e.g. *Clostridium*,  
521 *Corynebacterium* and *Turicibacter*), acetate (e.g. *Bacillus*, *Paenibacillus* and  
522 *Corynebacterium*), formate (e.g. *Lachnoclostridium*, *Romboutsia* and  
523 *Caproiciproducens*), butyrate (*Bacillus*, *Clostridium* and *Caproiciproducens*) and H<sub>2</sub>  
524 (*Clostridium* and *Romboutsia*) metabolisms took place. The figure shows a complex  
525 ecosystem where different key players act sequentially to use the available resources  
526 and maximize their own fitness. In fact, the proliferation of LAB and acetic acid  
527 bacteria (AAB) led to the transformation of complex carbohydrates, while lowering the  
528 pH and assuring an anaerobic condition. The activity of LAB and AAB was jeopardized  
529 by the exhaustion of resources and the accumulation of by-products such as lactate and  
530 acetate, which are used as carbon and energy sources by lactate-consuming HPB,  
531 acetate-consuming HPB and butyrate-producing bacteria. The cooperative interaction  
532 between LAB, AAB and HPB has been previously observed in the gut microbiota,  
533 where the conversion of lactate to butyrate is one of the important factors for  
534 maintaining homeostasis in the gastrointestinal tract (Moens et al., 2016). The pH is a  
535 key factor for H<sub>2</sub> production through lactate fermentation in dark fermentation systems  
536 (Juang et al., 2011). Wu and colleagues (2012) reported the range of pH for maximizing  
537 H<sub>2</sub> production from lactate and acetate, which was between 5.5 and 6. The measured pH  
538 in our bioreactors was slightly higher than this range. The final pH in the bioreactors  
539 might be one of the reasons for low H<sub>2</sub> production in our OMW-fermentation system.  
540

541 **4. Conclusion**

542 High-throughput sequencing and metabolic profile analyses revealed the substrate  
543 conversion routes that take place in an OMW-fermentation system that is designed for  
544 H<sub>2</sub> production. Lactate fermentation was the main H<sub>2</sub>-producing route. During the  
545 fermentation process, lactate and acetate were consumed, while H<sub>2</sub> and butyrate were  
546 being produced. Lactate conversion to butyrate through the generation of pyruvate  
547 proceeded via either butyrate kinase or butyryl-CoA: acetate-CoA transferase. Overall,  
548 these findings showed the synergy among LAB, AAB and HPB, which complex  
549 interactions produced H<sub>2</sub> through the recycling of the electron carriers ferredoxin and  
550 NADH via the PFOR pathway.

551

552 **Supplementary materials**

553 E-supplementary data of this work can be found in online version of the paper.

554

555 **Funding**

556 This work was partially supported by Fondazione Cariplo, VOLAC- Valorization of  
557 OLive oil wastes for sustainable production of biocide-free Antibiofilm Compounds,  
558 grant no. 2017-0977.

559

560 **References**

- 561 1. Aguilera, M., Monteoliva-Sánchez, M., Suárez, A., Guerra, V., Lizama, C.,  
562 Bannasar, A., Ramos-Cormenzana, A., 2001. *Paenibacillus jamilae* sp. nov., an  
563 exopolysaccharide-producing bacterium able to grow in olive-mill wastewater.  
564 Int. J. Syst. Evol. Microbiol. 51, 1687–1692. [https://doi.org/10.1099/00207713-](https://doi.org/10.1099/00207713-51-5-1687)  
565 [51-5-1687](https://doi.org/10.1099/00207713-51-5-1687)
- 566 2. Aguilera, M., Quesada, M.T., del Águila, V.G., Morillo, J.A., Rivadeneyra,  
567 M.A., Ramos-Cormenzana, A., Monteoliva-Sánchez, M., 2008. Characterisation  
568 of *Paenibacillus jamilae* strains that produce exopolysaccharide during growth  
569 on and detoxification of olive mill wastewaters. Bioresour. Technol. 99, 5640–  
570 5644. <https://doi.org/10.1016/j.biortech.2007.10.032>
- 571 3. Aharonov-Nadborny, R., Tsechansky, L., Raviv, M., Graber, E.R., 2018.  
572 Mechanisms governing the leaching of soil metals as a result of disposal of olive  
573 mill wastewater on agricultural soils. Sci. Total Environ. 630, 1115–1123.  
574 <https://doi.org/10.1016/j.scitotenv.2018.02.270>
- 575 4. American Public Health Association (APHA) Standard Methods for the  
576 Examination of Water and Wastewater (21st ed.), American Public Health  
577 Association Water Works Association, American Water Environment  
578 Federation, Washington, DC (2005)
- 579 5. Baghchehsaraee, B., Nakhla, G., Karamanev, D., Margaritis, A., 2009. Effect of  
580 extrinsic lactic acid on fermentative hydrogen production. Int. J. Hydrogen  
581 Energy 34, 2573–2579. <https://doi.org/10.1016/j.ijhydene.2009.01.010>
- 582 6. Bolyen, E., Rideout, J.R., Dillon, M.R., Bokulich, N.A., Abnet, C.C., Al-  
583 Ghalith, G.A., Alexander, H., Alm, E.J., Arumugam, M., Asnicar, F., Bai, Y.,  
584 Bisanz, J.E., Bittinger, K., Brejnrod, A., Brislawn, C.J., Brown, C.T., Callahan,  
585 B.J., Caraballo-Rodríguez, A.M., Chase, J., Cope, E.K., Da Silva, R., Diener, C.,

586 Dorrestein, P.C., Douglas, G.M., Durall, D.M., Duvallet, C., Edwardson, C.F.,  
587 Ernst, M., Estaki, M., Fouquier, J., Gauglitz, J.M., Gibbons, S.M., Gibson, D.L.,  
588 Gonzalez, A., Gorlick, K., Guo, J., Hillmann, B., Holmes, S., Holste, H.,  
589 Huttenhower, C., Huttley, G.A., Janssen, S., Jarmusch, A.K., Jiang, L., Kaehler,  
590 B.D., Kang, K. Bin, Keefe, C.R., Keim, P., Kelley, S.T., Knights, D., Koester, I.,  
591 Kosciolk, T., Kreps, J., Langille, M.G.I., Lee, J., Ley, R., Liu, Y.X., Loftfield,  
592 E., Lozupone, C., Maher, M., Marotz, C., Martin, B.D., McDonald, D., McIver,  
593 L.J., Melnik, A. V., Metcalf, J.L., Morgan, S.C., Morton, J.T., Naimey, A.T.,  
594 Navas-Molina, J.A., Nothias, L.F., Orchanian, S.B., Pearson, T., Peoples, S.L.,  
595 Petras, D., Preuss, M.L., Pruesse, E., Rasmussen, L.B., Rivers, A., Robeson,  
596 M.S., Rosenthal, P., Segata, N., Shaffer, M., Shiffer, A., Sinha, R., Song, S.J.,  
597 Spear, J.R., Swafford, A.D., Thompson, L.R., Torres, P.J., Trinh, P., Tripathi,  
598 A., Turnbaugh, P.J., Ul-Hasan, S., van der Hooft, J.J.J., Vargas, F., Vázquez-  
599 Baeza, Y., Vogtmann, E., von Hippel, M., Walters, W., Wan, Y., Wang, M.,  
600 Warren, J., Weber, K.C., Williamson, C.H.D., Willis, A.D., Xu, Z.Z., Zaneveld,  
601 J.R., Zhang, Y., Zhu, Q., Knight, R., Caporaso, J.G., 2019. Reproducible,  
602 interactive, scalable and extensible microbiome data science using QIIME 2.  
603 Nat. Biotechnol. 37, 852-857. <https://doi.org/10.1038/s41587-019-0209-9>  
604 7. Boonsaen, P., Kinjo, M., Sawanon, S., Suzuki, Y., Koike, S., Kobayashi, Y.,  
605 2018. Partial characterization of phylogeny, ecology and function of the  
606 fibrolytic bacterium *Ruminococcus flavefaciens* OS14, newly isolated from the  
607 rumen of swamp buffalo. Anim. Sci. J. 89, 377-385.  
608 <https://doi.org/10.1111/asj.12927>  
609 8. Cabrol, L., Marone, A., Tapia-Venegas, E., Steyer, J.P., Ruiz-Filippi, G., Trably,  
610 E., 2017. Microbial ecology of fermentative hydrogen producing bioprocesses:  
611 Useful insights for driving the ecosystem function. FEMS Microbiol. Rev. 41,



- 612 158-181. <https://doi.org/10.1093/femsre/fuw043>
- 613 9. de Sá, L.R.V., Faber, M. de O., da Silva, A.S.A., Cammarota, M.C., Ferreira-  
614 Leitão, V.S., 2020. Biohydrogen production using xylose or  
615 xylooligosaccharides derived from sugarcane bagasse obtained by hydrothermal  
616 and acid pretreatments. *Renew. Energy* 146, 2408–2415.  
617 <https://doi.org/10.1016/j.renene.2019.08.089>
- 618 10. Dermeche, S., Nadour, M., Larroche, C., Moulti-Mati, F., Michaud, P., 2013.  
619 Olive mill wastes: Biochemical characterizations and valorization strategies.  
620 *Process Biochem.* 48, 1532–1552. <https://doi.org/10.1016/j.procbio.2013.07.010>
- 621 11. Doula, M.K., Moreno-Ortego, J.L., Tinivella, F., Inglezakis, V.J., Sarris, A.,  
622 Komnitsas, K., 2017. Olive mill waste: Recent advances for the sustainable  
623 development of olive oil industry, Olive Mill Waste: Recent Advances for  
624 Sustainable Management. Elsevier Inc. 29-56. <https://doi.org/10.1016/B978-0-12-805314-0.00002-9>
- 625
- 626 12. Duncan, S.H., Louis, P., Flint, H.J., 2004. Lactate-utilizing bacteria, isolated  
627 from human feces, that produce butyrate as a major fermentation product. *Appl.*  
628 *Environ. Microbiol.* 70, 5810-5817. <https://doi.org/10.1128/AEM.70.10.5810-5817.2004>
- 629
- 630 13. Feng, K., Li, H., Zheng, C., 2018. Shifting product spectrum by pH adjustment  
631 during long-term continuous anaerobic fermentation of food waste. *Bioresour.*  
632 *Technol.* 270, 180–188. <https://doi.org/10.1016/j.biortech.2018.09.035>
- 633 14. Filannino, P., Bai, Y., Di Cagno, R., Gobbetti, M., Gänzle, M.G., 2015.  
634 Metabolism of phenolic compounds by *Lactobacillus* spp. during fermentation  
635 of cherry juice and broccoli puree. *Food Microbiol.* 46, 272-279.  
636 <https://doi.org/10.1016/j.fm.2014.08.018>
- 637 15. Fuess, L.T., Ferraz, A.D.N., Machado, C.B., Zaiat, M., 2018. Temporal

- 638 dynamics and metabolic correlation between lactate-producing and hydrogen-  
639 producing bacteria in sugarcane vinasse dark fermentation: The key role of  
640 lactate. *Bioresour. Technol.* 247, 426-433.  
641 <https://doi.org/10.1016/j.biortech.2017.09.121>
- 642 16. García-Depraect, O., Valdez-Vázquez, I., Rene, E.R., Gómez-Romero, J.,  
643 López-López, A., León-Becerril, E., 2019. Lactate- and acetate-based  
644 biohydrogen production through dark co-fermentation of tequila vinasse and  
645 nixtamalization wastewater: Metabolic and microbial community dynamics.  
646 *Bioresour. Technol.* 282, 236-244.  
647 <https://doi.org/10.1016/j.biortech.2019.02.100>
- 648 17. Gerritsen, J., Fuentes, S., Grievink, W., van Niftrik, L., Tindall, B.J.,  
649 Timmerman, H.M., Rijkers, G.T., Smidt, H., 2014. Characterization of  
650 *Romboutsia ilealis* gen. nov., sp. nov., isolated from the gastro-intestinal tract of  
651 a rat, and proposal for the reclassification of five closely related members of the  
652 genus *Clostridium* into the genera *Romboutsia* gen. nov., *Intestinibacter* gen.  
653 nov., *Terrisporobacter* gen. nov. and *Asaccharospora* gen. nov. *Int. J. Syst.*  
654 *Evol. Microbiol.* 64, 1600-1616. <https://doi.org/10.1099/ijms.0.059543-0>
- 655 18. Ghimire, A., Frunzo, L., Pontoni, L., d'Antonio, G., Lens, P.N.L., Esposito, G.,  
656 Pirozzi, F., 2015. Dark fermentation of complex waste biomass for biohydrogen  
657 production by pretreated thermophilic anaerobic digestate. *J. Environ. Manage.*  
658 152, 43-48. <https://doi.org/10.1016/j.jenvman.2014.12.049>
- 659 19. Ghimire, A., Sposito, F., Frunzo, L., Trably, E., Escudié, R., Pirozzi, F., Lens,  
660 P.N.L., Esposito, G., 2016. Effects of operational parameters on dark  
661 fermentative hydrogen production from biodegradable complex waste biomass.  
662 *Waste Manag.* 50, 55–64. <https://doi.org/10.1016/j.wasman.2016.01.044>
- 663 20. Greening, C., Geier, R., Wang, C., Woods, L.C., Morales, S.E., McDonald,

- 664 M.J., Rushton-Green, R., Morgan, X.C., Koike, S., Leahy, S.C., Kelly, W.J.,  
665 Cann, I., Attwood, G.T., Cook, G.M., Mackie, R.I., 2018. Alternative hydrogen  
666 uptake pathways suppress methane production in ruminants. bioRxiv 486894.  
667 <https://doi.org/10.1101/486894>
- 668 21. Gutiérrez, N., Garrido, D., 2019. Species deletions from microbiome consortia  
669 reveal key metabolic interactions between gut microbes. mSystems 4, e00185-  
670 19. <https://doi.org/10.1128/msystems.00185-19>
- 671 22. Ikeda-Ohtsubo, W., Brugman, S., Warden, C.H., Rebel, J.M.J., Folkerts, G.,  
672 Pieterse, C.M.J., 2018. How can we define “optimal microbiota?”: a  
673 comparative review of structure and functions of microbiota of animals, fish,  
674 and plants in agriculture. Front. Nutr. 5, 90.  
675 <https://doi.org/10.3389/fnut.2018.00090>
- 676 23. Ince, O., Akyol, Ç., Ozbayram, E.G., Tural, B., Ince, B., 2020. Enhancing  
677 methane production from anaerobic co-digestion of cow manure and barley:  
678 Link between process parameters and microbial community dynamics. Environ.  
679 Prog. Sustain. Energy. 39. <https://doi.org/10.1002/ep.13292>
- 680 24. Jin, Y., Lin, Y., Wang, P., Jin, R., Gao, M., Wang, Q., Chang, T.C., Ma, H.,  
681 2019. Volatile fatty acids production from saccharification residue from food  
682 waste ethanol fermentation: Effect of pH and microbial community. Bioresour.  
683 Technol. 292, 121957. <https://doi.org/10.1016/j.biortech.2019.121957>
- 684 25. Juang, C.P., Whang, L.M., Cheng, H.H., 2011. Evaluation of bioenergy recovery  
685 processes treating organic residues from ethanol fermentation process.  
686 Bioresour. Technol. 102, 5394-5399.  
687 <https://doi.org/10.1016/j.biortech.2010.10.069>
- 688 26. Kanchanasuta, S., Prommeenate, P., Boonapatcharone, N., Pisutpaisal, N., 2017.  
689 Stability of *Clostridium butyricum* in biohydrogen production from non-sterile

- 690 food waste. *Int. J. Hydrogen Energy* 42, 3454–3465.  
691 <https://doi.org/10.1016/j.ijhydene.2016.09.111>
- 692 27. Klein, A.M., Bohannan, B.J.M., Jaffe, D.A., Levin, D.A., Green, J.L., 2016.  
693 Molecular evidence for metabolically active bacteria in the atmosphere. *Front.*  
694 *Microbiol.* 7, 1–11. <https://doi.org/10.3389/fmicb.2016.00772>
- 695 28. Kothari, R., Kumar, V., Pathak, V. V., Ahmad, S., Aoyi, O., Tyagi, V. V., 2017.  
696 A critical review on factors influencing fermentative hydrogen production.  
697 *Front. Biosci. - Landmark* 22, 1195–1220. <https://doi.org/10.2741/4542>
- 698 29. Langille, M.G.I., Zaneveld, J., Caporaso, J.G., McDonald, D., Knights, D.,  
699 Reyes, J.A., Clemente, J.C., Burkepille, D.E., Vega Thurber, R.L., Knight, R.,  
700 Beiko, R.G., Huttenhower, C., 2013. Predictive functional profiling of microbial  
701 communities using 16S rRNA marker gene sequences. *Nat. Biotechnol.* 31,  
702 814–821. <https://doi:10.1038/nbt.2676>.
- 703 30. Lin, H., Wu, X., Hu, B., Zhu, J., 2014. microbial electrochemical systems for  
704 agro-industrial wastewater remediation and renewable products generation: a  
705 review. *Elyns J. Microbes* 01, 1–20. <https://doi.org/10.19104/amb.2014.101>
- 706 31. Łukajtis, R., Hołowacz, I., Kucharska, K., Glinka, M., Rybarczyk, P., Przyjazny,  
707 A., Kamiński, M., 2018. Hydrogen production from biomass using dark  
708 fermentation. *Renew. Sustain. Energy Rev.* 91, 665-694.  
709 <https://doi.org/10.1016/j.rser.2018.04.043>
- 710 32. Maaroff, R.M., Md Jahim, J., Azahar, A.M., Abdul, P.M., Masdar, M.S.,  
711 Nordin, D., Abd Nasir, M.A., 2019. Biohydrogen production from palm oil mill  
712 effluent (POME) by two stage anaerobic sequencing batch reactor (ASBR)  
713 system for better utilization of carbon sources in POME. *Int. J. Hydrogen*  
714 *Energy.* 44, 3395-3406. <https://doi.org/10.1016/j.ijhydene.2018.06.013>
- 715 33. Maharaj, B.C., Mattei, M.R., Frunzo, L., Hullebusch, E.D. va., Esposito, G.,

- 716 2019. ADM1 based mathematical model of trace element complexation in  
717 anaerobic digestion processes. *Bioresour. Technol.* 276, 253–259.  
718 <https://doi.org/10.1016/j.biortech.2018.12.064>
- 719 34. Matsumoto, M., Nishimura, Y., 2007. Hydrogen production by fermentation  
720 using acetic acid and lactic acid. *J. Biosci. Bioeng.* 103, 236–241.  
721 <https://doi.org/10.1263/jbb.103.236>
- 722 35. Meftah, O., Guergueb, Z., Braham, M., Sayadi, S., Mekki, A., 2019. Long term  
723 effects of olive mill wastewaters application on soil properties and phenolic  
724 compounds migration under arid climate. *Agric. Water Manag.* 212, 119–125.  
725 <https://doi.org/10.1016/j.agwat.2018.07.029>
- 726 36. Moens, F., Verce, M., De Vuyst, L., 2017. Lactate- and acetate-based cross-  
727 feeding interactions between selected strains of lactobacilli, bifidobacteria and  
728 colon bacteria in the presence of inulin-type fructans. *Int. J. Food Microbiol.*  
729 241, 225–236. <https://doi.org/10.1016/j.ijfoodmicro.2016.10.019>
- 730 37. Moscoviz, R., Trably, E., Bernet, N., Carrère, H., 2018. The environmental  
731 biorefinery: State-of-the-art on the production of hydrogen and value-added  
732 biomolecules in mixed-culture fermentation. *Green Chem.* 20, 3159–3179.  
733 <https://doi.org/10.1039/c8gc00572a>
- 734 38. Purohit, A., Rai, S.K., Chownk, M., Sangwan, R.S., Yadav, S.K., 2017.  
735 Xylanase from *Acinetobacter pittii* MASK 25 and developed magnetic cross-  
736 linked xylanase aggregate produce predominantly xylopentose and xylohexose  
737 from agro biomass. *Bioresour. Technol.* 244, 793–799.  
738 <https://doi.org/10.1016/j.biortech.2017.08.034>.
- 739 39. Pintucci, C., Padovani, G., Giovannelli, A., Traversi, M.L., Ena, A., Pushparaj,  
740 B., Carlozzi, P., 2015. Hydrogen photo-evolution by *Rhodospseudomonas*  
741 *palustris* 6A using pre-treated olive mill wastewater and a synthetic medium

742 containing sugars. *Energy Convers. Manag.* 90, 499–505.  
743 <https://doi.org/10.1016/j.enconman.2014.11.045>

744 40. Rapin, A., Pattaroni, C., Marsland, B.J., Harris, N.L., 2017. Microbiota analysis  
745 using an Illumina MiSeq platform to sequence 16S rRNA genes. *Curr. Protoc.*  
746 *Mouse Biol.* 7, 100-129. <https://doi.org/10.1002/cpmo.29>

747 41. Rocha, C., Soria, M.A., Madeira, L.M., 2017. Steam reforming of olive oil mill  
748 wastewater with in situ hydrogen and carbon dioxide separation –  
749 Thermodynamic analysis. *Fuel* 207, 449–460.  
750 <https://doi.org/10.1016/j.fuel.2017.06.111>

751 42. Scoma, A., Bertin, L., Fava, F., 2013. Effect of hydraulic retention time on  
752 biohydrogen and volatile fatty acids production during acidogenic digestion of  
753 dephenolized olive mill wastewaters. *Biomass and Bioenergy* 48, 51–58.  
754 <https://doi.org/10.1016/j.biombioe.2012.10.028>

755 43. Spasiano, D., Luongo, V., Race, M., Petrella, A., Fiore, S., Apollonio, C.,  
756 Pirozzi, F., Fratino, U., Piccinni, A.F., 2019. Sustainable bio-hydrothermal  
757 sequencing treatment for asbestos-cement wastes. *J. Hazard. Mater.* 364, 256–  
758 263. <https://doi.org/10.1016/j.jhazmat.2018.10.025>

759 44. Tao, Y., Hu, X., Zhu, X., Jin, H., Xu, Z., Tang, Q., Li, X., 2016. Production of  
760 butyrate from lactate by a newly isolated *Clostridium* sp. BPY5. *Appl. Biochem.*  
761 *Biotechnol.* 179, 361-374. <https://doi.org/10.1007/s12010-016-1999-6>

762 45. Vavouraki, A.I., Zakoura, M. V., Dareioti, M.A., Kornaros, M., 2019.  
763 Biodegradation of polyphenolic compounds from olive mill wastewaters  
764 (OMW) during two-stage anaerobic co-digestion of agro-industrial mixtures.  
765 *Waste and Biomass Valorization*. <https://doi.org/10.1007/s12649-019-00887-4>

766 46. Wu, C.W., Whang, L.M., Cheng, H.H., Chan, K.C., 2012. Fermentative  
767 biohydrogen production from lactate and acetate. *Bioresour. Technol.* 113, 30-6.

768 <https://doi.org/10.1016/j.biortech.2011.12.130>

769 47. Yang, G., Wang, J., 2018. Synergistic biohydrogen production from flower  
770 wastes and sewage sludge. *Energy and Fuels* 32, 6879–6886.  
771 <https://doi.org/10.1021/acs.energyfuels.8b01122>

772 48. Yang, G., Wang, J., 2019. Changes in microbial community structure during  
773 dark fermentative hydrogen production. *Int. J. Hydrogen Energy* 44, 25542–  
774 25550. <https://doi.org/10.1016/j.ijhydene.2019.08.039>

775 49. Yang, G., Yin, Y., Wang, J., 2019. Microbial community diversity during  
776 fermentative hydrogen production inoculating various pretreated cultures. *Int. J.*  
777 *Hydrogen Energy* 44, 13147–13156.  
778 <https://doi.org/10.1016/j.ijhydene.2019.03.216>

779 50. Yin, Y., Wang, J., 2016. Changes in microbial community during biohydrogen  
780 production using gamma irradiated sludge as inoculum. *Bioresour. Technol.*  
781 200, 217–222. <https://doi.org/10.1016/j.biortech.2015.10.027>

782

783

784 **Figure and table Captions**

785 **Figure 1.** (A) Alpha diversity indices of the microbial communities during the  
786 fermentation process. (B) Taxonomic classification of the dominant bacterial groups  
787 over time in the OMW fermentation reactors. Only bacteria with relative abundances >  
788 1.0% were represented. Different letters indicate statistically significant differences at  $p$   
789 < 0.05. T0: inoculum; T3: the initial stage of H<sub>2</sub> production; T5: the rapid stage of H<sub>2</sub>  
790 production; T8: the end of the dark fermentation.

791

792 **Figure 2.** Ecological networks based on Pearson correlation analysis between the  
793 dominant bacterial groups. Shaded boxes show significant correlation at  $p < 0.05$ .

794

795 **Figure 3.** Time-course profile of cumulative biogas (A-D), pH (E) and organic acids (F-  
796 I) produced during the fermentation of OMW. Biogas production parameters (the gas  
797 production potential  $H_0$  (mL), the maximum gas production rate  $R$  (mL d<sup>-1</sup>), the lag-  
798 phase time  $\lambda$  (d) and the determination coefficient  $R^2$ ) measured by the modified  
799 Gompertz model are reported in panels A-D. Different letters indicate statistically  
800 significant differences at  $p < 0.05$ . T0: inoculum; T3: the initial stage of H<sub>2</sub> production;  
801 T5: the rapid stage of H<sub>2</sub> production; T8: the end of the dark fermentation.

802

803 **Figure 4.** Correlation between bacterial groups, time and process performance  
804 indicators by principal component analyses (PCA). T0: inoculum; T3: the initial stage  
805 of H<sub>2</sub> production; T5: the rapid stage of H<sub>2</sub> production; T8: the end of the dark  
806 fermentation

807

808 **Figure 5.** (A) Heat map of the predicted relative abundances of genes that encodes the  
809 key enzymes involved in lactate, acetate, formate and butyrate metabolisms. T0:



810 inoculum; T3: the initial stage of H<sub>2</sub> production; T5: the rapid stage of H<sub>2</sub> production;  
811 T8: the end of the dark fermentation. (B) The main metabolic routes for the H<sub>2</sub>  
812 production from lactate acetate, formate and butyrate. Thicker lines indicated the  
813 principal metabolic route based on relative gene abundance.

814

815 **Figure 6:** The predicted genus-level phylotypes that contribute to genes encoding for  
816 key enzymes involved in the production and consumption of lactate, acetate, formate,  
817 butyrate, and hydrogen.